Volume 12
Number 8
August 2025
Pages 3811–4140

Environmental Science Nano

rsc.li/es-nano

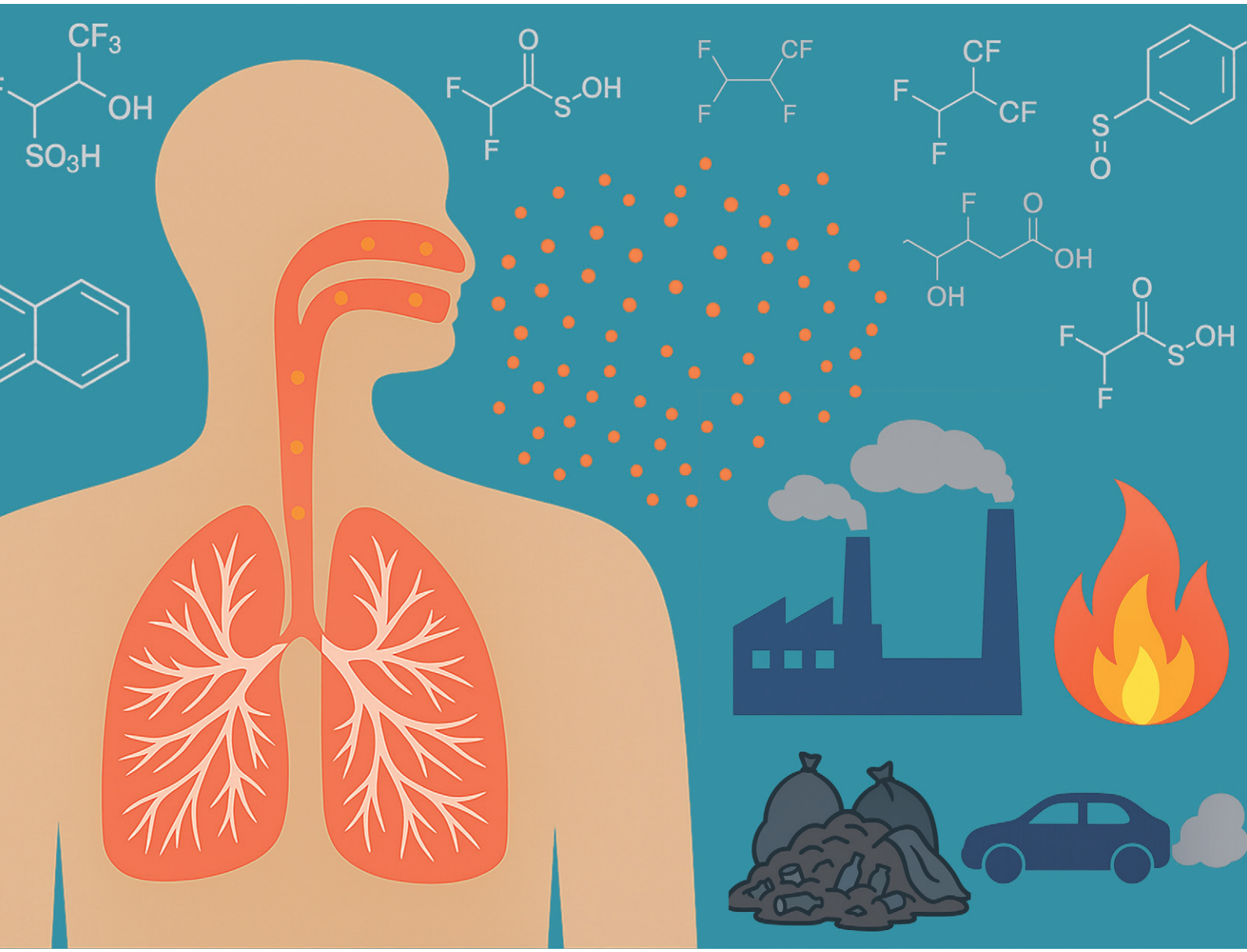

ISSN 2051-8153

ROYAL SOCIETY OF CHEMISTRY

PAPER
Iseult Lynch, Antreas Afantitis *et al.*
LungDepo: modelling the regional particle deposition in the human lung *via* the Enalos Cloud platform

Environmental Science Nano

ROYAL SOCIETY OF CHEMISTRY

PAPER

View Article Online
View Journal | View Issue

Cite this: *Environ. Sci.: Nano*, 2025, **12**, 3921

LungDepo: modelling the regional particle deposition in the human lung *via* the Enalos Cloud platform†

Dimitris G. Mintis, [ab] Dimitra-Danai Varsou, [bc] Panagiotis D. Kolokathis, [bc] Andreas Tsoumanis, [ab] Georgia Melagraki, [d] Johannes P. Seif, [e] Alejandro J. del Real, [ef] Iseult Lynch *[bg] and Antreas Afantitis *[abc]

Received 16th March 2025,
Accepted 3rd July 2025

DOI: 10.1039/d5en00299k

rsc.li/es-nano

This work presents the development of *LungDepo*, a freely accessible online web application hosted on the Enalos Cloud platform (**https://enaloscloud.novamechanics.com/proplanet/lungdeposition** or **https://enaloscloud.novamechanics.com/insight/lungdeposition/**), which enables users to simulate particle deposition in the human lung across the head airway, the tracheobronchial and the alveolar (pulmonary) regions based on the aerodynamic diameter of inhaled particles. The *LungDepo* web-based tool offers two modelling approaches: the International Commission on Radiological Protection (ICRP) model and the multiple path particle dosimetry (MPPD) model, to simulate regional particle deposition and assess inhalation toxicity risk. In addition to modeling the fractional regional particle deposition based on the two implemented models, *LungDepo* offers the computation of the regional deposited mass (mg) and the computation of the regional lung surface area covered by deposited particles (m^2) providing statistical analyses of the relative contributions of coarse (2.5–10.0 micron), fine (<2.5 micron) and ultrafine (<0.1 micron) particles. The web-based tool includes predefined modelling scenarios for various particle-bound substances or co-pollutants such as polycylic aromatic hydrocarbons (PAHs) or per- and polyfluoroalkyl substances (PFAS) and micro-sized engineered materials, along with provision for the inclusion of user-defined particle size distributions. The integration of an application programming interface (API) and the development of an intuitive graphical user interface (GUI) facilitate data exchange and integration with external environmental and regulatory toxicity models by simplifying complex tasks and broadening the tool's applicability for diverse users in environmental research, monitoring, and regulatory activities.

Environmental significance

Every human breath may expose individuals to a toxic cocktail of ultrafine particles and engineered nanomaterials that are silently deposited in the human lungs. In this study, *LungDepo* is introduced as a free-to-use web application that uses dosimetry models to quantify the deposition of airborne particles within the human respiratory tract. The tool provides statistical analyses of the contributions of coarse (2.5–10.0 μm), fine (<2.5 μm), and ultrafine (<0.1 μm) particles. Designed for non-programmers, *LungDepo* is accessible to a wide audience and can potentially support broader regulatory frameworks for assessing human inhalation toxicity and safeguarding public health.

1 Introduction

Air pollution results from the release of harmful substances into the atmosphere, originating from a variety of sources, including industrial emissions, vehicle exhaust, and natural events.[1–4] Air pollution is responsible for approximately 9–12 million deaths annually on a global scale.[5,6] The World Health Organization (WHO) identifies six principal air pollutants: particle pollution (particulate matter), ground-level ozone, carbon monoxide, sulfur oxides, nitrogen oxides, and lead.[5,7] These pollutants can be broadly categorized based on their physical state into gases

[a] *NovaMechanics Ltd., Nicosia 1070, Cyprus.*
E-mail: afantitis@novamechanics.com; Tel: +357 99048039
[b] *Entelos Institute, Larnaca 6059, Cyprus*
[c] *NovaMechanics MIKE, Piraeus 18545, Greece*
[d] *Division of Physical Sciences and Applications, Hellenic Military Academy, Vari 16672, Greece*
[e] *IDENER, 41300 Sevilla, Spain*
[f] *Department of Systems and Automation, University of Seville, 41092 Seville, Spain*
[g] *School of Geography, Earth and Environmental Sciences, University of Birmingham, Birmingham B15 2TT, UK*

† Electronic supplementary information (ESI) available: ESI file is included, providing a comprehensive analysis of the outcomes generated using the *LungDepo* web-tool. See DOI: **https://doi.org/10.1039/d5en00299k**

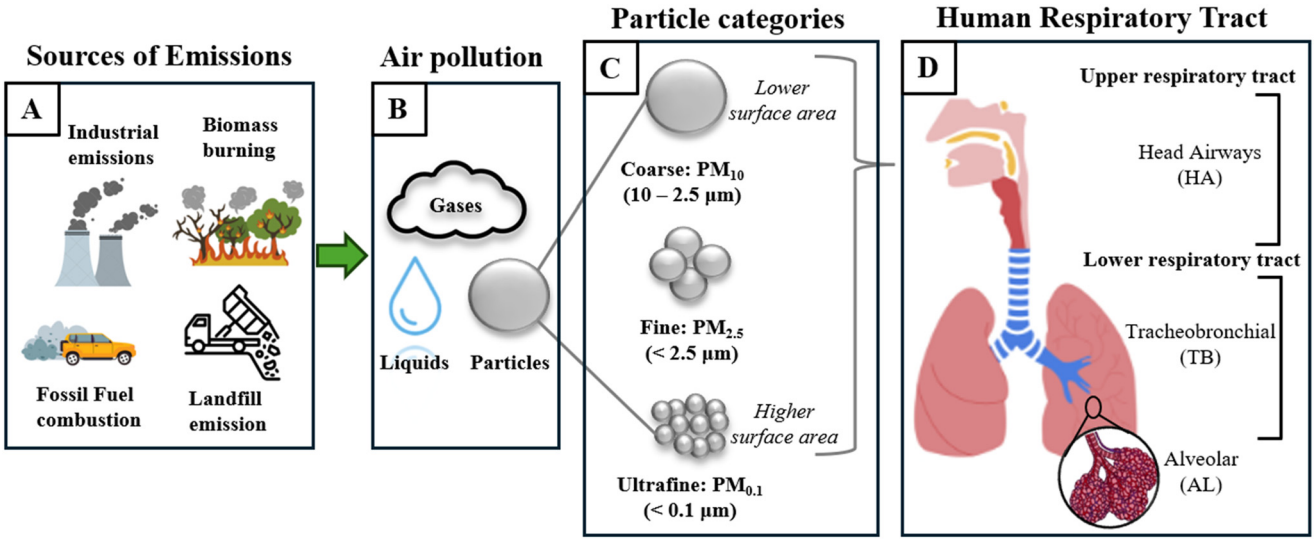

Fig. 1 (A) Key sources of air pollution from both anthropogenic and natural activities, (B) categorized into gases, volatile liquids, and particulate matter of (C) varying sizes, highlighting their penetration potential in the (D) human respiratory tract, distinguishing between the upper and lower respiratory tract.

(*e.g.*, ozone, carbon monoxide, nitrogen oxides, sulfur oxides), volatile liquids (*e.g.*, certain organic compounds contributing to ozone formation), and particulate matter (solid or liquid particles suspended in the air, such as fine dust, soot, and aerosols) (Fig. 1B). Among these, particulate matter (PM) has emerged as the most critical air/environmental pollutant, as it is associated with the highest mortality and morbidity rates due to a range of health issues, including cardiovascular and pulmonary diseases, arrhythmias, coughing, chest discomfort and dyspnea.[2,8–16] PM consists of aerosol particles suspended in the air that may be composed of either liquid or solid particulate matter.[17] These particles may be formed in the atmosphere as a result of chemical reactions among various pollutants,[5] or result from a range of both anthropogenic (road dust, waste-water treatment plants, landfills, construction sites, mining, office equipment, cooking *etc.*)[18–21] and natural sources (soil, plants, volcanoes, forest fires, sea spray *etc.*)[2,22] (Fig. 1A). Based on aerodynamic diameter, PM is categorized into three size fractions as coarse (PM_{10}, 2.5–10.0 μm),[5,23] fine ($PM_{2.5}$, <2.5 μm)[23] and ultrafine ($PM_{0.1}$, <0.1 μm)[24] (Fig. 1C). Fine and ultrafine particles are likely to enter the lower airways upon inhalation, causing detrimental respiratory health effects. Particles larger than 10 μm are mostly filtered by the nasal and upper respiratory tract[25,26] (Fig. 1D).

Understanding the deposition of inhaled particulate matter in the different regions of the respiratory tract is crucial for evaluating, quantifying and predicting inhalation toxicity. The chemical composition of PM is primarily carbonaceous with contributions from inorganic ions (including sulphates, nitrates and metal oxides) and volatile and semi-volatile organic compounds such as polycyclic aromatic hydrocarbons (PAHs), polychlorinated biphenyls (PCBs), organochlorine pesticides (OCPs), and per- and polyfluoroalkyl substances (PFAS),[27–29] which can alter biological activity and contribute to carcinogenic, neurotoxic, and endocrine-disrupting effects.[30–34] Fine and ultrafine particles remain airborne longer, penetrate deeper into the lungs, and often carry highly reactive transition metals and oxidized organics, enhancing their toxicity.[35] Furthermore, microparticles or micro-sized engineered materials and their agglomerates with aerodynamic diameters between 0.1 and 100 μm such as zinc oxide (ZnO),[36,37] iron oxide (Fe_2O_3),[38] titanium dioxide (TiO_2),[39] aluminum oxide (Al_2O_3),[40] copper oxide (Cu_2O),[41] cobalt oxide (Co_3O_4)[41] and nickel hydroxide ($Ni(OH)_2$)[42] may pose additional inhalation hazards due to their ability to penetrate deep into the respiratory tract. Engineered micro-sized materials are applied in various industrial and consumer products.[39] Consequently, it is crucial to evaluate the effects of inhalation exposure, particularly in terms of pulmonary toxicity, that may arise as a result of their very small dimensions.[39]

From a morphological perspective, the human respiratory system consists of two distinct structural regions. The first consists of the extrathoracic airways, termed as the head airways (HA) consisting of the nose, mouth, pharynx and larynx. The second consists of the tracheobronchial (TB) airway trees and the alveolar (AL) regions[43] (Fig. 1D). Deposition in the HA and TB regions act as barriers to safeguard the AL region, which constitutes the air–blood barrier, from potential irritation or harmful particles.[44] In the AL region, where the airway walls lacks a mucus layer, deposited insoluble particles are effectively cleared by the alveolar macrophages.[43] However, soluble particles deposited in the AL region may dissolve and pass through the alveolar membranes, entering the systemic circulation.[43,45] Numerous factors affect the regional deposition of particles within the human lungs, primarily dependent on an individuals' pulmonary physiology such as breathing patterns and lung geometry.[46,47] Additionally, the physicochemical

characteristics of inhaled particles, such as their size, size distribution, density, shape, charge, surface properties, hygroscopicity (ability to absorb moisture from the surrounding air) and the interactions between particles and pulmonary surfactant play a critical role.[35,48–50] Of these factors, the size of inhaled particles is considered as the key predominant factor affecting the fate and regional deposition of particles in the human lungs.[51] Coarser size particles (PM_{10}) tend to lodge in the throat and/or the bronchi, whereas fine and ultrafine particles can travel deeper into the airways of the respiratory tract, reaching the alveoli, binding with proteins that support (opsonising) or hamper (disopsonising) recognition by macrophages and influence crossing of anatomical barriers, and penetrating into the bloodstream.[2,8,52]

The experimental determination of particle deposition within the human respiratory tract poses significant challenges in both *in vivo* and *in vitro* studies. *In vivo* studies are ethically problematic, while *in vitro* models have significant limitations in accurately replicating realistic physiological conditions.[53] To overcome these limitations, particle dosimetry models have been extensively developed over the past decades to calculate the regional deposition patterns of inhaled aerosols.[54–56] It is still challenging however, to accurately measure and quantify analytically the deposition of particles in the respiratory tract due to the intricate interplay between the structural morphology of lungs (that differs between individuals) and the hydrodynamic flow field within the airways, which constantly undergoes dynamic changes.[44] According to Hofmann,[57] existing particle dosimetry models are categorized based on lung morphometry and mathematical modelling techniques into semi-empirical models,[58–60] one-dimensional cross-section or "trumpet" models,[61–64] mechanistic models,[65–70] and computational fluid and particle dynamics (CFPD)-based models.[71–75] Among the most widely used particle dosimetry models are two semi-empirical models that combine (first-principle) mechanistic frameworks with experimental (empirical) data:[57,58,76] the ICRP66 model developed by the International Committee of Radiological Protection (ICRP) in 1994 (ref. 58) (which has since been updated to ICRP130),[59] and the NCRP model developed by the National Council on Radiation Protection and Measurements (NCRP) in the USA, in 1997.[60] Additionally, mechanistic models such as the deterministic asymmetric branching model, also known as the multiple pathway particle dosimetry (MPPD) model, introduced in 2001,[77,78] and the stochastic asymmetric branching model, referred to as IDEAL (inhalation, deposition and exhalation of aerosols in the lung), developed between 1990 and 1992,[69,70,79] which derive deposition fractions directly from classical flow equations. The clearance mechanisms of particles are not discussed here, as they are beyond the scope of the present work.

The objective of this work is to introduce a publicly accessible web application, *LungDepo*, designed to facilitate users including policy-makers, public health professionals and risk assessors in employing the ICRP and MPPD models for the quantification of particle deposition within the three anatomical compartments of the human lungs: the head airways (HA), the tracheobronchial region (TB), and the alveolar region (AL). Designing and developing a web application in the context of inhalation toxicity is essential for providing accessible and efficient tools that can be utilized by a wide range of users without the need for advanced mathematical or programming skills. Well-designed graphical user interfaces (GUI) are crucial for enabling users with limited technical expertise to navigate and apply complex models for assessing inhalation risks. This accessibility promotes broader use of the models, enabling researchers, healthcare professionals, and policymakers to efficiently conduct evaluations and make informed decisions. Additionally, incorporating application programming interfaces (API) capabilities enhances the flexibility of the web application, allowing it to integrate with external datasets, automate processes, and support the implementation of customized workflows. This facilitates collaboration across different research domains and accelerates innovation in the design of safer materials and substances and evaluation of the potential impacts of mitigation measures to reduce exposures to particles. *LungDepo* is hosted on the Enalos Cloud platform facilitating its integration with other freely accessible web applications within the framework of nano-informatics, including several human health related models such as the integrated approach to testing and assessment (IATA) for lung exposure and toxicity.[80–82] The Enalos Cloud platform also offers access to several other models including *NanoBioAccumulate*,[83] which simulates nanomaterial uptake and elimination in aquatic and soil invertebrates; *MicroPlasticFate*,[84] which provides the dynamic and steady-state modeling of the environmental fate of micro- and nanoplastics across key environmental scales and compartments; and *UANanoDock*,[85] which predicts protein adsorption onto nanoparticles. Beyond nano-informatics, the Enalos Cloud platform also hosts web applications in cheminformatics,[86,87] and machine learning,[88,89] providing a versatile infrastructure for developing, deploying, and accessing predictive models in materials and life sciences.

The *LungDepo* web application presented in this study is specifically designed to offer a user-friendly GUI that supports the application of complex models for computing the mass deposition (of particles themselves or based on concentrations of adsorbed co-pollutants), the lung surface area covered by deposited particles and the relative contributions of inhaled particulates classified by their size (coarse, fine and ultrafine) in the various regions of the human lungs. As regulators and industry increasingly shift towards the implementation of safe and sustainable by design (SSbD) principles for the design of chemicals and materials, the *LungDepo* web application provides valuable insights into how new materials can be engineered to reduce harmful effects on human health as well as visualizing the impacts of altering the particle size distributions through specific emissions mitigation measures. Additionally, *LungDepo* features predefined scenario models to simulate the deposition of several airborne substances and micro-

sized engineered materials in the human lungs depending on the breathing frequency and concentration of airborne particles.

2 Particle (aerosol) deposition models

2.1 ICRP model

The ICRP model, integrated within the *LungDepo* web application employs the simplified deposition equations proposed by Hinds in 1999.[44] These equations are applicable for the calculation of fractional deposition of particles in the size range from 0.001 to 100 μm. Several studies have employed the Hinds equations for the ICRP model to study the respiratory deposition of aerosols.[90,91]

This model provides calculations for the deposition efficiency of inhaled particles across three distinct regions of the respiratory tract: the head airways (HA), the tracheobronchial region (TB), and the alveolar region (AR). The deposition efficiency of particles across these three distinct regions is calculated as follows:

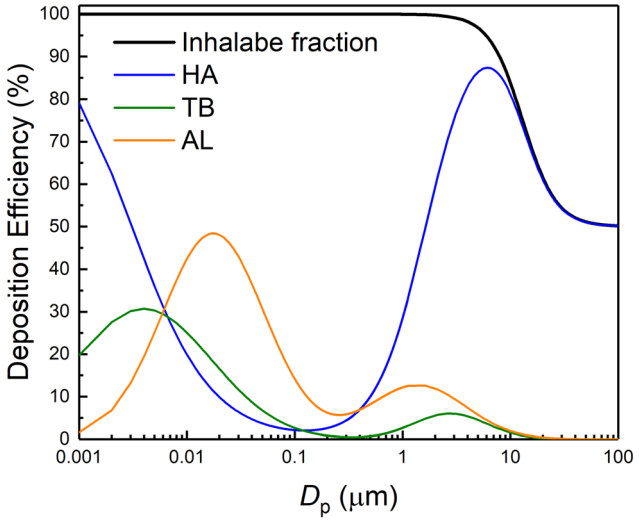

Fig. 2 Deposition efficiency (fraction) computed based on the simplified equations proposed by Hinds[44] for the ICRP model, plotted against the aerodynamic particle diameter in the range 0.001–100 μm.

$$\mathrm{DE}_{\mathrm{HA},i} = \mathrm{IF}_i \cdot \left[\frac{1}{1 + \exp\left(6.84 + 1.183 \ln D_{\mathrm{p},i}\right)} + \frac{1}{1 + \exp\left(0.924 + 1.885 \ln D_{\mathrm{p},i}\right)} \right] \quad (1)$$

$$\mathrm{DE}_{\mathrm{TB},i} = \left(\frac{0.00352}{D_{\mathrm{p},i}} \right) \cdot \left[\exp\left(-0.234 \left(\ln D_{\mathrm{p},i} + 3.40 \right)^2 \right) + 63.9 \exp\left(-0.819 \left(\ln D_{\mathrm{p},i} - 1.61 \right)^2 \right) \right] \quad (2)$$

$$\mathrm{DE}_{\mathrm{AL},i} = \left(\frac{0.0155}{D_{\mathrm{p},i}} \right) \cdot \left[\exp\left(-0.416 \left(\ln D_{\mathrm{p},i} + 2.84 \right)^2 \right) + 19.11 \exp\left(-0.482 \left(\ln D_{\mathrm{p},i} - 1.362 \right)^2 \right) \right] \quad (3)$$

$$\mathrm{IF}_i = 1 - 0.5 \cdot \left[1 - \frac{1}{1 + 0.00076 \times {D_{\mathrm{p},i}}^{2.8}} \right] \quad (4)$$

where $D_{\mathrm{p},i}$ (μm) is the aerodynamic diameter of the particle in each size fraction and IF_i is the inhalable fraction of all particles.

Fig. 2, presents the analytical calculation of the deposition efficiency (fraction) in the three regions of the human lung as a function of the aerodynamic particle size, ranging from 0.001 μm to 100 μm, using the simplified equations proposed by Hinds[44] for the ICRP model. The *x*-axis, which represents the aerodynamic diameter of particles, is displayed on a logarithmic scale. As shown in Fig. 2, the ICRP model suggests that particles with aerodynamic diameter of less than 10 μm are inhaled at nearly 100%. In contrast, particles larger than 10 μm in diameter exhibit a significantly reduced inhalable fraction, becoming lodged within the head airways of the human lung. Ultrafine particles with aerodynamic diameter of less than 0.1 μm ($\mathrm{PM}_{0.1}$) exhibit significant deposition efficiencies, reaching up to 50% in the alveolar region and approximately 30% in the tracheobronchial regions.

2.2 MPPD model

The MPPD model, integrated within the *LungDepo* web application, is specifically tailored to align with human symmetric lung geometry as proposed by Yeh and Schum.[65] This model is the recommended default human geometry by the U.S. Environmental Protection Agency (EPA).[92] The functional residual capacity (FRC), the volume of air present in the lungs at the end of passive expiration in a 70 kg average-sized male, is set at 3300 mL, while the upper respiratory tract (URT) volume is designated at 50 mL. The inhalation pathway is specified as nasal, with inhaled particles considered to be spherical in shape, spanning a size range from 0.001 to 100 μm. The breathing parameters are defined as 12 breathes per minute, a tidal volume (the volume of gas inhaled and exhaled with each breath) of 625 mL, and an inspiratory fraction (inspiratory capacity/total lung capacity) of 0.5.

Fig. 3, presents the analytical calculation of the deposition efficiency (fraction) for particles deposited in the three

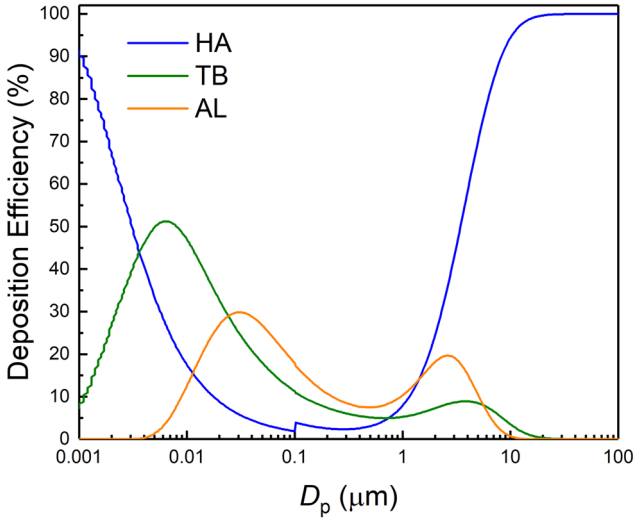

Fig. 3 Deposition efficiency (fraction) computed using the MPPD model version 3.04, developed by Applied Research Associates Inc.,[78,93] plotted against the aerodynamic particle diameter in the range 0.001–100 μm.

regions of the human lungs using the MPPD model version 3.04, developed by Applied Research Associates Inc.[78,93] based on the conditions described in the previous paragraph. The analysis reveals three notable discrepancies between the outcomes of the ICRP model and the MPPD model. Firstly, the ICRP model estimates the AL deposition efficiency for ultrafine particles to be approximately 50%, whereas the MPPD model yields a lower estimate of approximately 30%. Secondly, regarding the deposition efficiency for ultrafine particles in the TB region, the MPPD model estimates the efficiency to be approximately 50%, contrasting with the ICRP model's lower estimate of around 30%. According to the ICRP model, the inhalation efficiency for particles with an aerodynamic diameter up to 100 μm declines to approximately 60%. In contrast, the MPPD model suggests that all particles within this diameter range (100%) continue to be inhaled.

2.3 Deposition mass flow rate

The total mass deposition rate, $m_{\text{deposition}}$ (mg h^{-1}), is estimated by:

$$m_{\text{deposition}} = c_{\text{particles}} \cdot V_{\text{particles}} \cdot t_{\text{exposute}} \cdot \sum_i (f_i \cdot \text{DE}_i) \quad (5)$$

where $c_{\text{particles}}$ is the concentration of particles (mg m^{-3}), $V_{\text{particles}}$ is the human breathing rate (m^3 h^{-1}), t_{exposure} is the exposure duration (measured in hours), f_i is the normalized probability density for particle size $D_{p,i}$ (expressed as decimal fraction, *i.e.*, 10% is represented as 0.1) and DE_i is the particle deposition efficiency calculated using either the ICRP or MPPD model.[94]

2.4 Lung surface area on which particles are deposited

The *LungDepo* web application integrates the computation of the total surface area of the lung covered by deposited particles (measured in m^2), to assess the extent of particle coverage across the HA, TB and AL regions.

The total deposited surface area of particles, $A_{\text{deposition}}$, is calculated as:

$$A_{\text{deposition}} = \sum_i (N_i \cdot A_i) \quad (6)$$

where N_i is the number of particles (deposited) in the specific region of the lung and A_i is the surface area (m^2) for a given particle aerodynamic diameter, $D_{p,i}$, respectively.

The number N_i of particles deposited for a given particle aerodynamic diameter, $D_{p,i}$ is given by:

$$N_i = \frac{m_{\text{deposition}}}{m_i} \quad (7)$$

where m_i is the mass for a given particle aerodynamic diameter (measured in mg), given by:

$$m_i = \frac{\pi}{6} \cdot \rho \cdot D_{p,i}^3 \quad (8)$$

where ρ is the density of the particles (g cm^{-3}).

The surface area, A_i, assuming the particles are spherical, is given by:

$$A_i = \pi \cdot D_{p,i}^2 \quad (9)$$

3 The *LungDepo* web application

The *LungDepo* web application is designed with a user-centric approach and is developed utilizing the ZK framework – an open-source Ajax web application framework implemented in Java.[95] This web application is hosted on the Enalos Cloud platform (**https://enaloscloud.novamechanics.com/proplanet/lungdeposition/** or **https://enaloscloud.novamechanics.com/insight/lungdeposition/**)[96] and is freely accessible to all users without cost or login requirements, as it is provided as freeware (free-to-use software with closed-source code).

Fig. 4 presents the graphical user interface (GUI) of the *LungDepo* web application. In this example, the chosen model is the ICRP, accompanied by a predefined scenario for the particle size distribution of PFAS in particulate matter collected from a coastal area, as reported in the study by Lin *et al.*[91] Once the model and scenario related to particle size distribution are selected, two intuitive graphical plots are generated. The first plot represents the normalized probability density of the aerodynamic diameter size distribution of the particulate matter. The second plot shows the deposition efficiency, expressed as a fraction, across the relevant range of particle sizes. In the example shown, the concentration of exposure to particulate matter is set at 6.644×10^{-7} mg m^{-3}, with a respiratory volume rate reflective of a female in a sitting position, set at 0.39 m^3 h^{-1}. The exposure duration is defined as 3600 seconds. By selecting the 'enable

Fig. 4 Display of the web interface of the *LungDepo* tool for a scenario in which the ICRP model is selected alongside a predefined particle size distribution. The results show the distribution of the different size fractions of the particles in the three regions of the lung.

advanced options' check box, the user can specify the density of particles, which is set to 1 g cm^{-3} in this example. Also, the user can define the total surface area of the HA, TB and AL regions, measured in m^2. Upon selecting the 'calculate dose' button, users can obtain the lung regional deposited doses of particles, measured in milligrams (mg) and as a percentage (%). Here, the percentage represents the fraction of the total deposited mass that occupies the surface area of a specific lung region relative to the total mass deposited across the entire lung. Additionally, users can retrieve the deposited dose of particles per regional lung surface area (mg m^{-2}), the surface area (of the lung region) covered by deposited particles (m^2) and the ratio of the surface area covered by deposited particles to the total regional lung area, expressed as percentage (%). The output also includes the relative contributions of particles classified by size in the three different regions of the human lung, measured in percentage. This classification includes coarse particles larger than 2.5 μm, fine particles less than 2.5 μm, and ultrafine particles smaller than 0.1 μm. Additionally, there is an option to download the results *via* the 'Download Dose Data' button.

The user may choose from a dropdown menu that includes the ICRP and MPPD models. Additionally, for the scenario pertaining to particle size distribution, users can select from a range of predefined examples representing various substances that may be constituents of particulate matter. These substances include[91] perfluorobutanoic acid (PFBA),[91] perfluorobutane sulfonate (PFBS),[91] corn starch,[97] chitosan,[98] glycerol,[99] zinc oxide (ZnO),[100] acetic acid,[101] silane-based[102] and siloxane-based[103] substances, 2-octenylsuccinic anhydride,[104] sodium alginate,[105] alkyl ketene dimers (AKDs)[106] and polycyclic aromatic hydrocarbons (PAHs)[107] substances as reported in previous studies. Users have the option to upload a custom scenario as well pertaining to the size distribution of the substance of interest within particulate matter. Additionally, for the respiratory volume rate, users may choose from predefined scenarios established by the ICRP model, which takes into account gender as well as varying activity levels, such as sitting, light exercise, or heavy exercise.[43] To support broader applicability, *LungDepo* includes a step-by-step user guide, which is directly available within the web application interface, explaining how to upload a custom particle size distribution in .txt format and how to manually define all relevant input parameters, including particle concentration, respiratory volume rate, exposure duration, particle density, and lung region surface areas to ensure that users can apply easily *LungDepo* to a wide variety of compounds and exposure scenarios.

The *LungDepo* web application incorporates a representational state transfer (REST) application programming interface (API) that enhances both its functionality and usability. This is shown in Fig. 5. The functionality of the 'POST' and 'GET' requests for

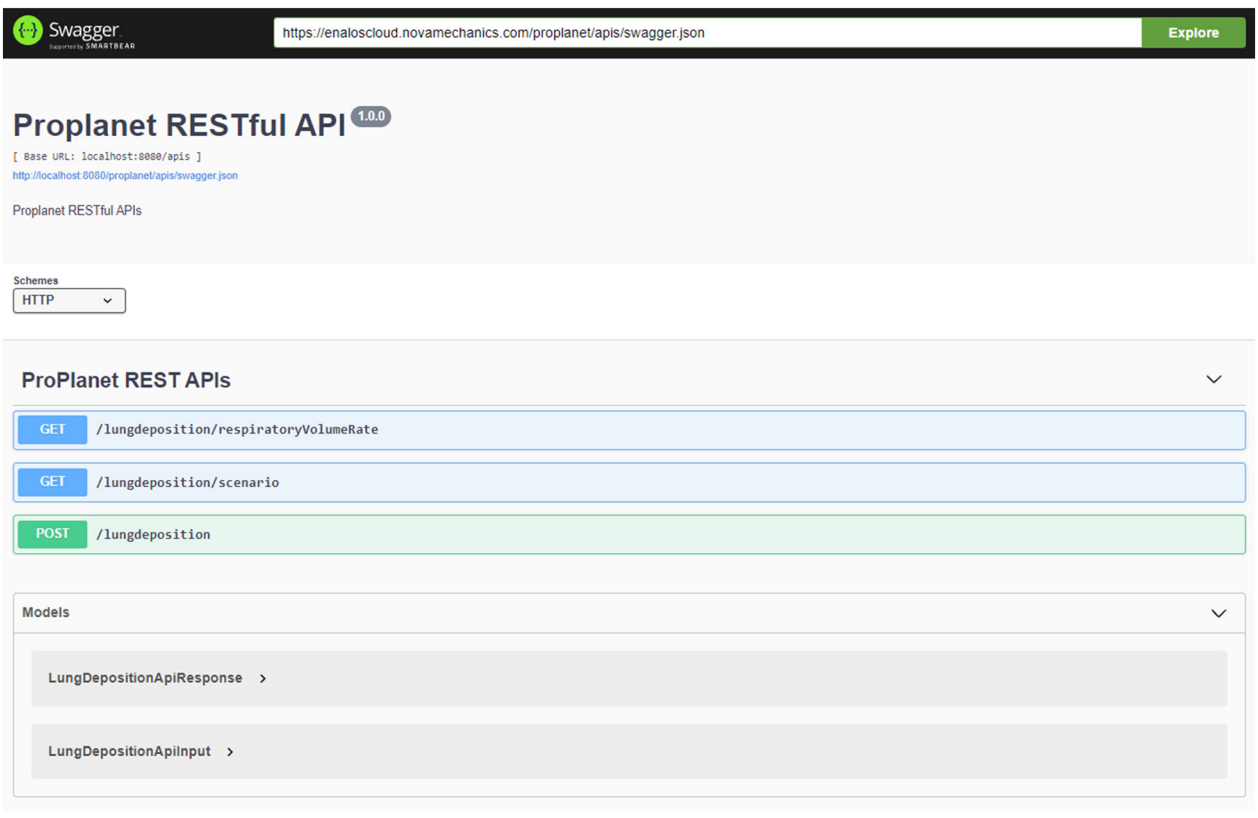

Fig. 5 *LungDepo* is available through a REST API to enable programmatic access and integration with other models, tools and into an IATA for hazard and risk assessment.

the endpoints **https://enaloscloud.novamechanics.com/proplanet/apis/lungdeposition**, **https://enaloscloud.novamechanics.com/proplanet/apis/lungdeposition/scenario** and **https://enaloscloud.novamechanics.com/proplanet/apis/lungdeposition/respiratoryVolumeRate**, respectively, were tested using Postman (see Fig. S1, S3 and S4†). The same tests were performed using Swagger. The API documentation is publicly accessible *via* the Swagger user interface (see Fig. 5) at **https://enaloscloud.novamechanics.com/proplanet/swagger-ui/index.html#/** and the underlying specification at **https://enaloscloud.novamechanics.com/proplanet/apis/swagger.json**. Fig. S2† demonstrates the use of Swagger to perform a '/lungdeposition' POST request, using the same input data as shown in Fig. S1† (which used Postman), confirming consistency of the output across tools. This testing ensured that the expected responses were returned for each request type. In section S2 of the ESI,† robustness tests for the '/lungdeposition' POST query are presented by submitting extreme input scenarios. Specifically, two high-value and two low-value test cases were constructed using exaggerated concentrations, nanoparticle densities and tidal surface areas across the alveolar, tracheobronchial, and head airway regions, using both the ICRP and MPPD models implemented in *LungDepo*. All tests were performed using Postman and, in every case, the API successfully returned results, confirming the robustness and reliability of its implementation under a wide range of input conditions. A REST API allows the *LungDepo* web application to interact with external systems and services in a standardized way, facilitating the exchange of data between the application and other tools, databases, or platforms. This means that users can access the application's features programmatically, enabling integration with broader research ecosystems and allowing for automation of tasks, such as data input, analysis, and reporting. Additionally, the REST API provides scalability and flexibility, allowing different users – whether researchers, developers, or public health professionals – to customize their workflows by integrating the web application into their existing systems. For instance, researchers can automate the analysis of large-scale datasets to simulate particle deposition under various conditions or integrate *LungDepo* with other modeling tools to enhance the breadth of their inhalation toxicity studies.

Furthermore, a REST API facilitates collaboration by enabling multiple users to access the same application from different locations or systems, allowing for shared research efforts and cross-platform compatibility. This makes the application more adaptable to different research needs, supporting a wide range of use cases – from routine regulatory assessments to advanced scientific research in inhalation toxicology. By providing a flexible and interoperable interface, a REST API significantly expands the reach and impact of the *LungDepo* web application, helping users make more informed decisions in evaluating inhalation toxicity, evaluating the impact of exposure mitigation measures such as air filtration, and designing materials by application of the SSbD principles. Integrating the *LungDepo* web application into the Enalos Cloud Platform further enhances its capabilities by allowing users to access other web applications hosted on the same platform, including the integrated approach to testing and assessment (IATA) for lung exposure and toxicity.[80–83] This integration fosters a collaborative environment where different tools can be used together to provide comprehensive insights and support multifaceted research efforts.

4 Case studies

4.1 Particle-bound PFAS

The ICRP and MPPD dosimetry models incorporated into the *LungDepo* web application are used to estimate the deposited doses and surface area on which inhaled particulate-bound per- and polyfluoroalkyl substances (PFAS) are deposited across the three distinct regions of the human lung. The relative contributions of inhaled PFAS associated with particles of different sizes are also computed. The predictions generated by *LungDepo* (using the input data from Lin *et al.*[91]), are compared with the findings reported by Lin *et al.*[91] to verify the accuracy and robustness of the ICRP and MPPD models as integrated within the web application.

Lin *et al.*[91] conducted extensive work quantifying the (normalized) particle size distribution of particle-bound PFAS and the sum concentrations of gaseous and particulate PFAS emitted from various reference sites, including wastewater treatment plants (WWTPs), landfills, coastal areas and natural reserve sites. They investigated collectively 49 PFAS and reported the particulate concentrations of each, measured in picograms of PFAS per cubic meter in the air (pg m^{-3}). The total concentrations were designated as Σ PFAS. The normalized distribution of total PFAS (Σ PFAS) on the different size fractions in the particulate matter, along with the total particulate concentrations of PFAS from different sampling locations as reported by Lin *et al.*,[91] have been included as predefined scenarios in the *LungDepo* web application. Among the predefined scenarios the normalized distributions of PFBA and PFBS are included, as obtained from the study of Lin *et al.*[91]

Fig. 6A, presents the predicted mass deposition rate (pg h^{-1}) of inhaled PFAS at or near a landfill site using the ICRP and MPPD models in *LungDepo* as compared to those calculated by Lin *et al.*[91] also using the ICRP model, while Fig. 6B presents the corresponding predicted mass deposition percentage (%) within the three distinct regions of the human lung calculated from the *LungDepo* model (this was not calculated by Lin *et al.*,[91] and is one of the new features of *LungDepo*). The corresponding figures for predicted exposures based on PFAS emissions at coastal and natural reserve sites and at WWTPs are provided in the supplemental information file (Fig. S9–S18†). These calculations were performed using the ICRP and MPPD dosimetry models integrated within the *LungDepo* web application, alongside the findings reported in the study by Lin *et al.*[91] to validate and verify the accuracy of the calculation outputs generated by the *LungDepo* web application. Lin *et al.*[91] used the simplified equations proposed by Hinds,[44] similar to our approach in this study, to calculate the mass deposition rate of inhaled PFAS based on the ICRP model. As can be observed

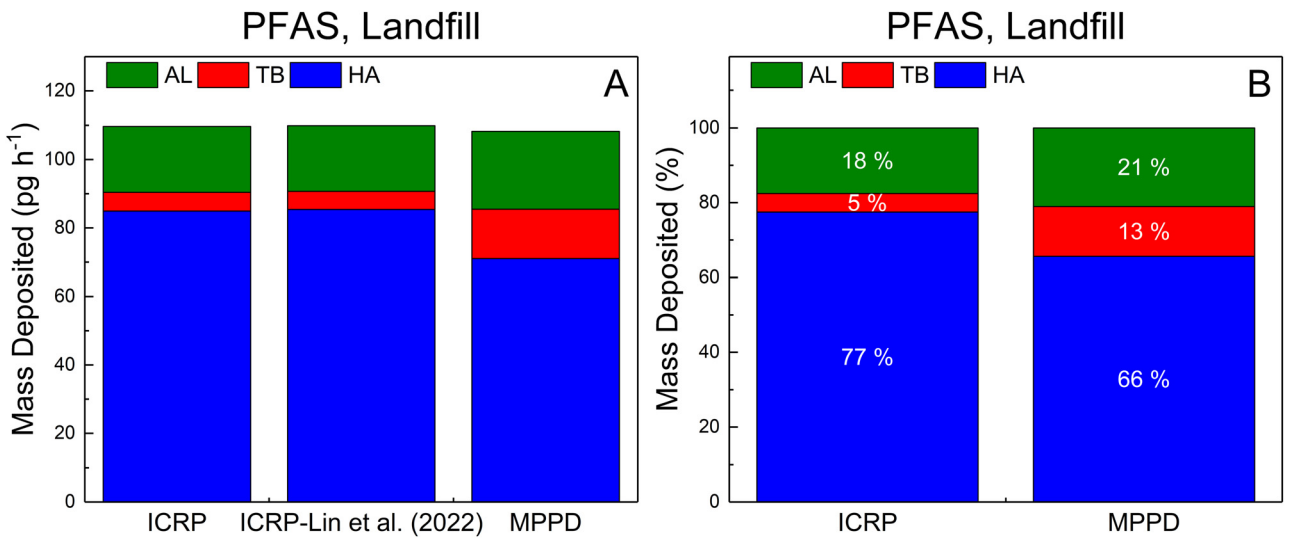

Fig. 6 Predictions of PFAS mass deposition at a landfill site in Hong Kong (based on input data from Lin *et al.*), computed using the ICRP and MPPD models integrated within *LungDepo*. (A) Deposition in pg h^{-1} compared with Lin *et al.*; (B) deposition in % of Σ PFAS, comparing ICRP and MPPD results.[91]

in Fig. 6A, the mass deposition rate calculated by the *LungDepo* web application is consistent with that reported by Lin *et al.*[91] thereby verifying the calculations performed in relation to the ICRP dosimetry model. The total mass of inhaled PFAS deposited, as estimated by both the ICRP and MPPD models, is approximately 110 pg h^{-1}. Specifically, the ICRP model predicts that the contributions to the HA, TB and AL region are roughly 77%, 5% and 18%, respectively. The MPPD model predicts that the contributions to the HA, TB and AL region are around 66%, 13% and 21%, respectively. These discrepancies are attributed to the different deposition efficiencies predicted by the two models, as shown in Fig. 2 and 3, respectively. The particle size distribution of the PFAS, as reported in the study by Lin *et al.*,[91] spanned from 0.08 to 25 μm. The distribution exhibited a peak at an aerodynamic diameter of 0.78 μm that corresponded to an inhalation probability of around 17%. It is evident from Fig. 2 and 3, that for particles with an aerodynamic diameter of approximately 0.78 μm, the ICRP model predicts slightly higher deposition efficiency in the HA, estimated at around 8%, compared to the 5% predicted by the MPPD model. Conversely, the deposition efficiency in the TB region, according to the ICRP model, is lower at approximately 1.7%, whereas the MPPD model predicts a value of around 5%. The differences predicted between the MPPD and ICRP models are minor and reflect the improved lung geometry in the MPPD model.

The total mass deposition and the contributions of different particle sizes of the particles to which the PFAS are bound, as calculated here using input data (on PFAS concentration and particle size distribution) retrieved from the study of Lin *et al.*,[91] are found to be consistent and comparable to the findings reported in the study of Guo *et al.*[90] Guo *et al.*,[90] reported that the mass deposition of eight PFAS within the human lungs, in the urban atmosphere of Shanghai, China is approximately 361 pg h^{-1}, indicating that the coarse PFAS particles contribute the most to the particle and PFAS load in the HA region. They also reported that PFAS particles with an aerodynamic diameter of less than 2.1 μm account for approximately 72.5% of the particle deposition in the AL region. This observation is comparable with the results presented here that demonstrated that fine and ultrafine particles contribute approximately 75–80% to the total deposition in the AL region.

The *LungDepo* web application offers further advanced analytical features for calculating the regional percentage contributions of the three distinct particle size categories (coarse, fine and ultrafine particles) as well as the computation of the deposited dose per regional area (mg m^{-2}) and evaluation of the percentage of the regional surface area on which particles have deposited relative to the total regional area (as a percentage) which can also be thought of as lung surface area in which effective lung function (*e.g.*, oxygen exchange) will likely be reduced. As can be seen in Fig. 7, both ICRP and MPPD models predict that coarse particles predominate in the HA region. In more detail, the MPPD model predicts this percentage to be slightly higher at around 89% of the total particle load, whereas ICRP predicts that coarse particles constitute around 74%. In the TB region, the MPPD model indicates that fine particles predominate corresponding to around 55% of the total particle load, whereas ICRP model indicates equal contribution between fine and coarse particles. In the AL region, both models predict that fine particles predominate this region with percentages around 60–65% and ultrafine particles contributing to around 15% of the total particle load here.

The predicted deposition dose per lung regional area of people in close proximity to the landfill, using the ICRP model, is found to be 5.03×10^{-5} mg m^{-2} in the HA region, 2.19×10^{-7} mg m^{-2} in the TB region and 2.34×10^{-9} mg m^{-2} in the AL region. The corresponding computations using the MPPD model yielded values of 4.24×10^{-5} mg m^{-2} in the HA

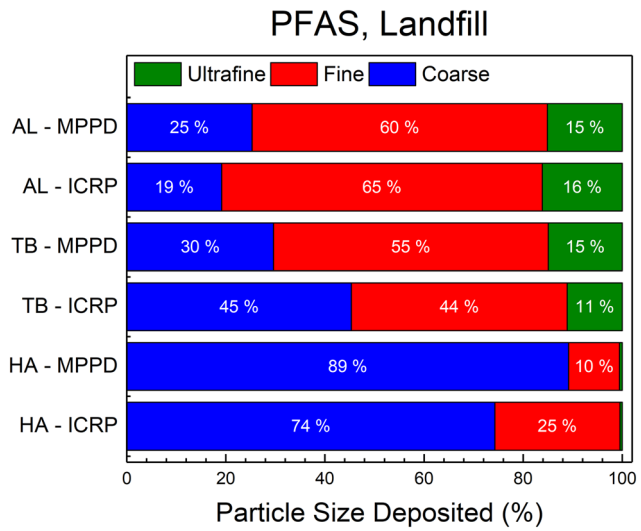

Fig. 7 Contributions (expressed as percentages of the Σ PFAS) of inhaled Σ PFAS associated with particles of different sizes (collected from a landfill site in Hong Kong by Lin *et al.*[91]) as calculated using the ICRP and MPPD models integrated within the *LungDepo* web application.

region, 5.84×10^{-7} mg m^{-2} in the TB region and 2.80×10^{-9} mg m^{-2} in the AL region. Although the predicted particles' coverage in the AL region is relatively low, in the order of 10^{-9} mg m^{-2}, as observed by both models, the computed mass of PFAS deposited in the AL region, which is found to be 20–25 pg h^{-1}, should be of concern regarding potential toxicological effects and health implications. While there are as yet limited health-based guidance values or limit values for individual or total PFAS concentrations in air, some suggestions are that annual exposure to PFOA (for example) should be limited to 0.0053 μg m^{-3}.[108] The European Food Safety Authority has advised a tolerable weekly intake (TWI) for total PFAS *via* food of 0.63 ng kg^{-1} from food and water for example.[109] In parallel, the U.S. Environmental Protection Agency (EPA) has set maximum contaminant levels (MCLs) in drinking water at or near zero for several PFAS compounds, including PFOA and PFOS, reflecting increasing concern over their health impacts and a shift toward more protective regulatory thresholds.[110]

4.2 Particle-bound total PAH

Polycyclic aromatic hydrocarbons (PAHs) represent another class of particle-bound organic compounds that may have significant adverse health effects upon human inhalation. The atmospheric presence of PAHs in both gas and particulate phases raises significant concerns, particularly due to the fine sizes of particle-bound PAHs that range from 0.1 to 10 μm (ref. 107 and 111) and which can penetrate deeply into the human respiratory system upon inhalation, potentially leading to significant health impacts. Furthermore, the concentrations of PAHs in the atmosphere are notably higher than those of PFAS, typically ranging from a few to hundreds of nanograms per cubic meter[112] Atmospheric particle-bound PAHs are primarily formed from the incomplete combustion of carbon-based materials[113–115] which are characterized by high biochemical persistence due to the existence of dense π electrons on the aromatic rings.[116,117]

Using the probability density size distribution as reported by Lv *et al.*[107] and the concentrations from the sum of 12 PAHs measured by Voliotis *et al.*[29] during cold (January–March 2013) and warm (May–July 2013) seasons at an urban traffic site in Thessaloniki (northern Greece), the mass deposition rate (ng h^{-1}) of particle-bound PAHs is calculated. The respiratory volume rate is set to 1.7 m^3 s^{-1} to be consistent with the study of Voliotis *et al.*[29] This volumetric rate corresponds to light activity levels in adults. The mass deposition rate is computed using the ICRP and MPPD models integrated within the *LungDepo* web application. The results were compared to those reported by Voliotis *et al.*,[29] who utilized the MPPD model with the stochastic lung option, applying a functional residual capacity (FRC) of 3389 mL. In contrast, the MPPD model integrated within the *LungDepo* web application is fitted based on a Yeh/Schum symmetric lung geometry model with an FRC of 3300 mL. Nevertheless, as presented in Fig. 8A and B respectively, the predicted outcomes from the MPPD model using *LungDepo* and the outcomes predicted by Voliotis are in close agreement during both cold and warm seasons. This comparison further assures the validity of the implementation of the MPPD model integrated within the *LungDepo* web application. The predicted outcome based on the ICRP model overestimates the mass deposition of particle-bound PAHs. This discrepancy as discussed previously is attributed to the different computations of deposition efficiency as evidenced in Fig. 2 and 3.

As can be seen in Fig. 8A and B, the mass deposition of particle-bound PAHs during the cold season is significantly higher, predicted to be approximately 18–20 ng h^{-1}, compared to the warm season, where deposition levels are predicted to be around 6–8 ng h^{-1}. This observation aligns with previous studies that reported higher concentrations of PAHs during cold seasons due to the increase from seasonal emission sources such as domestic heating *etc.*[118–122] and lower concentrations of PAHs during warm seasons due to the rise of temperature and concentrations of atmospheric oxidants such as ozone and radicals.[123–126]

4.3 Engineered microparticles (MPs)

In addition to the toxic organic compounds that can bound onto particulate matter, micro-sized engineered materials, with an aerodynamic diameter between 0.1 and 100 μm, have also been addressed as potential risks for environmental and occupational lung diseases following inhalation.[127] Engineered microparticles (MPs), which are classified as ultrafine particles (<0.1 μm), can be found in both indoor and outdoor aerosols.[128] Due to their small sizes, these particles can penetrate deep into the respiratory tract, potentially inducing pulmonary inflammation and other

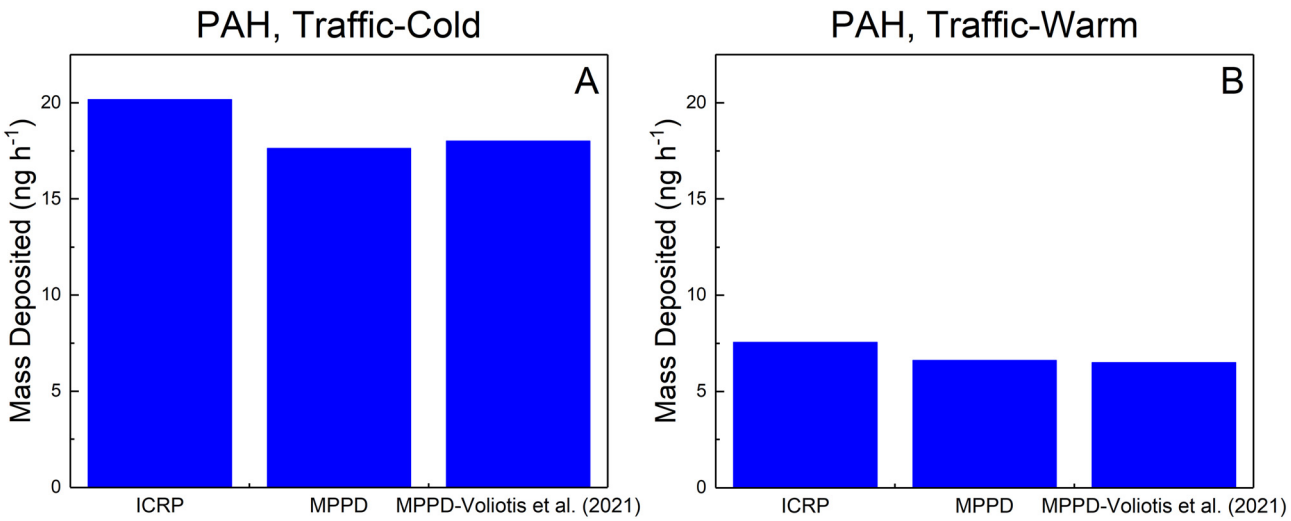

Fig. 8 Predictions of the mass deposition in human male adult lung measured in ng h^{-1} of PAHs during the cold season (A) and warm season (B) at an urban traffic site as computed using the ICRP and MPPD models integrated within *LungDepo* and compared against the previous study[29] (whose data was used as the input to the *LungDepo* model).[29]

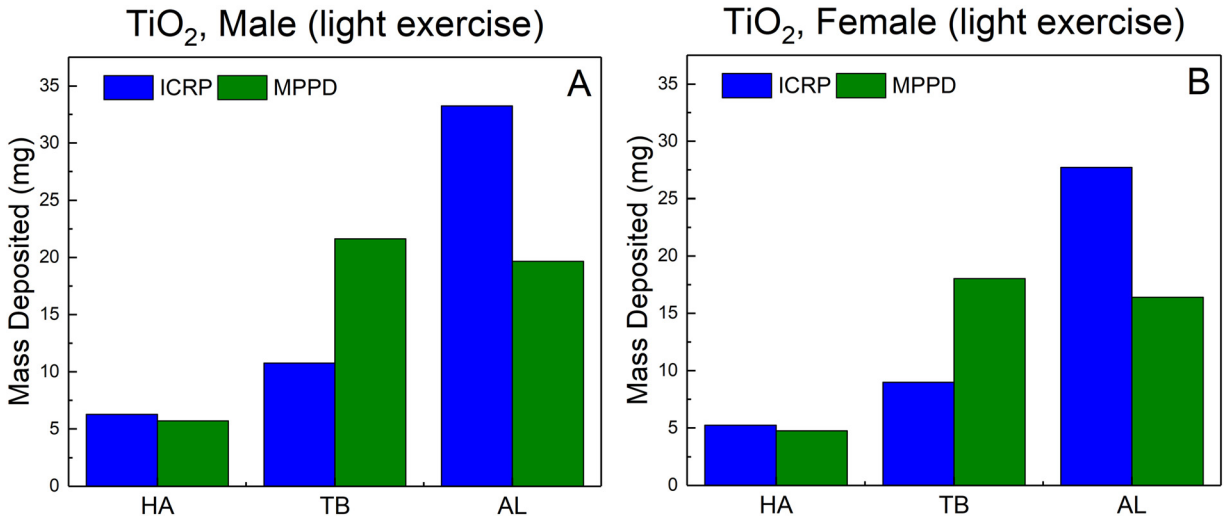

Fig. 9 Predictions of the mass deposition measured in ng h^{-1} of TiO_2 ultrafine particles, following the exposure of male (A) and female (B) workers to 22 nm TiO_2 under light exercise during an 8-hour work shift as computed using the ICRP and MPPD models integrated within *LungDepo*.

adverse health effects due to their ability to cross the air-lung barrier.[129,130]

A case study presented by Tsiros *et al.*[131] is used to examine the robustness and accuracy of the *LungDepo* web application to predict the mass of TiO_2 deposited in the three different human lung regions, following the exposure of female and male workers to 22 nm ultrafine TiO_2 particles under light exercise during an 8 hour work shift. Tsiros *et al.*,[131] employed the ICRP model using the Hinds approach,[44] and the MPPD model for assessing the risk exposure of female and male workers exposed to a concentration of 5.85 mg m^{-3} of TiO_2 ultrafine particles, considering a particle density (assuming spherical particles) of approximately 4.26 g cm^{-3} and a count median diameter of the particles (CMD) of 0.02 μm. Fig. 9A and B, present the mass deposition measured in mg calculated using the ICRP and MPPD models integrated within the *LungDepo* web application, following the exposure of a male or female, respectively to 22 nm ultrafine TiO_2 particles during an 8 hour work shift under light exercise. The ICRP model predicts that the largest mass of deposited TiO_2 microparticles is in the AL region, estimated at approximately 33 mg for males and 28 mg for females. This finding underscores the significant risk of pulmonary inflammation that may result from the 8 hour (workday) exposure to TiO_2 ultrafine particles, to both males and females. This observation is in perfect agreement with the calculations conducted by Tsiros *et al.*,[131] using the ICRP model. Using the MPPD model integrated within the *LungDepo* web application, it is observed that the predicted mass of TiO_2 deposited in the

alveolar (AL) region is also considerable, approximately 20 mg for males and 16 mg for females however, the largest accumulation of TiO_2 is predicted to be in the TB region. This discrepancy between the two models can be described through the calculation of deposition efficiency for particles measuring 0.022 μm, as illustrated in Fig. 2 and 3. It is noteworthy to state that although Tsiros *et al.*,[131] used the same lung geometry for MPPD model as used in this study, they considered variable exposure (30 minutes of active emissions per hour) in contrast to the MPPD model used in this study which was fitted based on a constant exposure scenario. This distinction largely explains the differences observed in the predictions yielded by the MPPD model integrated within the *LungDepo* web application and the predictions yielded by the MPPD model utilized by Tsiros *et al.*[131]

Using the advanced functionalities of the *LungDepo* web application, it has been observed that both the ICRP and MPPD models predict the surface area occupied by deposited particles per the regional area to be around 2–3% in the AL region, around 250% in the TB region and around 2500% in the HA region. These findings clearly indicate that inhalation of 22 nm ultrafine TiO_2 particles for 8 hours work shift, could potentially lead to significant pulmonary inflammation and other adverse health implications for both males and females.

4.4 Domain of applicability and user interaction

Following the presentation of the case studies demonstrating the applicability of the *LungDepo* web application for predicting the mass deposition of particle-bound toxic organic compounds and engineered micro-sized materials, it is important to note also that the web application integrates predefined (normalized) size distribution data for a variety of additional substances. This feature enables users to explore diverse scenarios involving various combinations of materials and chemicals, including perfluorobutyl sulfonate (PFBS), perfluorobutanoic acid (PFBA), corn starch, chitosan, glycerol, zinc oxide (ZnO), acetic acid, silane- and siloxane-based materials, 2-octenylsuccinic anhydride, sodium alginate, and alkyl ketene dimer (AKD). Furthermore, the web application accommodates the integration of user-defined particle size distributions, thereby enhancing the analytical flexibility of the tool. This signifies that the *LungDepo* web application can serve as a valuable tool for accurate and robust evaluation of the potential impacts of inhaled materials on the human respiratory tract by environmental regulatory agencies. Also, the web application can be utilized to investigate and assess the carcinogenic risks associated with inhalation exposure to these substances by calculating the inhalation cancer risk (ICR) metric.

Future extensions of *LungDepo* could include parameterisation of different lung sizes/breathing rates and functional residual capacities to cover also children and vulnerable populations (*e.g.*, pregnant women, the elderly, people with asthma, emphysema or other lung-related conditions, and obesity) which will influence both exposure and susceptibility to additional health effects arising from air pollution.[132,133]

5 Conclusions

This paper presents the *LungDepo* web application for the prediction of the mass deposition of inhaled particles and particle-associated organic pollutants within the respiratory tract. *LungDepo* is a freely accessible web application hosted on the Enalos Cloud platform (**https://enaloscloud.novamechanics.com/proplanet/lungdeposition** or **https://enaloscloud.novamechanics.com/insight/lungdeposition/**), which enables researchers to assess potential hazards and risks associated with the inhalation of particulate matter, toxic organic compounds bound to particles, micro-sized engineered materials or their combinations. The robustness and validity of *LungDepo*, utilizing either the ICRP or MPPD models, has been confirmed through several case studies comparing its predictions with the model calculations performed in previous studies,[29,90,91,107,131] including the mass deposition of particle-bound PFAS,[90,91] PAH aerosol[29,107] and micro-sized engineered material such as of TiO_2.[131] Its broad applicability is further demonstrated by integrating predefined case studies with (normalized) size distribution data for various substances, including perfluorobutyl sulfonate (PFBS), perfluorobutanoic acid (PFBA), corn starch, chitosan, glycerol, zinc oxide (ZnO), acetic acid, silane- and siloxane-based materials, 2-octenylsuccinic anhydride, sodium alginate, and alkyl ketene dimer (AKD). Further enhancements are planned to extend the range of pollutants and combinations available, and to enable tuning of the lung volume and residual capacity to allow modelling of the exposures and consequent risks of especially vulnerable individuals.

The enhanced user interaction and flexibility of the *LungDepo* web application is affirmed by its user-friendly GUI, which facilitates users with no programming knowledge to perform calculations using the ICRP and MPPD models for prediction of the mass deposition of inhaled particles and aerosols in the human lungs. The tool also features REST API integration that facilitates interaction with other web applications and software such as for integrated exposure, hazard and risk assessment, thereby promoting efficient data exchange and enhancing interoperability. This integration opens new opportunities for collaborative research and a thorough evaluation of inhalation toxicity, ultimately contributing to the design and development of inherently safer materials through application of the SSbD principles.

In this study, clearance mechanisms of deposited particles were not considered. To more accurately assess the risk from inhaled particles to human lungs, future work will integrate comprehensive physiologically-based pharmacokinetic (PBPK) models within *LungDepo*, such as the one presented in the work of Tsiros *et al.*[131] The inclusion of additional variants of MPPD models fitted to alternative lung geometric models, such as the Yeh/Schum 5-Lobe, the stochastic lung, the Weibel *etc.* will also be considered. Finally, the variable exposure conditions featured in the MPPD model version

3.04, developed by Applied Research Associates Inc.[78,93] will also be integrated within *LungDepo* in future upgrades.

Data availability

All data utilised in the manuscript is extracted from literature, and the curated datasets are in the process of being uploaded to the free-to-access NanoPharos database **https://db.nanopharos.eu/Queries/Datasets.zul**.

Author contributions

Conceptualization, D. M., D.-D. V.; methodology, D. M.; software, D. M., A. T.; supervision, G. M., J. S., I. L, A. A.; writing – original draft preparation, D. M.; writing – review and editing, D. M., D.-D. V., P. K., A. T., G. M., J. S., A. R., I. L., A. A.; funding acquisition, A. A.

Conflicts of interest

There are no conflicts to declare.

Acknowledgements

This research was funded by the European Union's Horizon 2020 research and innovation program *via* the PROPLANET project under grant agreement number 101091842 and the INSIGHT project under grant agreement number 101137742. The authors would like to thank Periklis Tsiros for the fruitful discussions, and his suggestions and advice for integrating additional statistical measures into the *LungDepo* web application to enable in-depth analysis of the regional deposition of particles in the human lungs.

References

1 A. S. Shah, J. P. Langrish, H. Nair, D. A. McAllister, A. L. Hunter, K. Donaldson, D. E. Newby and N. L. Mills, Global association of air pollution and heart failure: a systematic review and meta-analysis, *Lancet*, 2013, **382**, 1039–1048.
2 K.-H. Kim, E. Kabir and S. Kabir, A review on the human health impact of airborne particulate matter, *Environ. Int.*, 2015, **74**, 136–143.
3 L. B. Lave and E. P. Seskin, *Air pollution and human health*, RFF Press, 2013.
4 B. Brunekreef and S. T. Holgate, Air pollution and health, *Lancet*, 2002, **360**, 1233–1242.
5 I. Manisalidis, E. Stavropoulou, A. Stavropoulos and E. Bezirtzoglou, Environmental and health impacts of air pollution: a review, *Frontiers in public health*, 2020, **8**, 14.
6 R. J. Henning, Particulate matter air pollution is a significant risk factor for cardiovascular disease, *Curr. Probl. Cardiol.*, 2024, **49**, 102094.
7 WHO, **https://www.who.int/health-topics/air-pollution#tab=tab_1**, (accessed 25, 2024).
8 R. W. Atkinson, G. W. Fuller, H. R. Anderson, R. M. Harrison and B. Armstrong, Urban ambient particle metrics and health: a time-series analysis, *Epidemiology*, 2010, **21**, 501–511.
9 G. Cadelis, R. Tourres and J. Molinie, Short-term effects of the particulate pollutants contained in Saharan dust on the visits of children to the emergency department due to asthmatic conditions in Guadeloupe (French Archipelago of the Caribbean), *PLoS One*, 2014, **9**, e91136.
10 A. W. Correia, C. A. Pope III, D. W. Dockery, Y. Wang, M. Ezzati and F. Dominici, Effect of air pollution control on life expectancy in the United States: an analysis of 545 US counties for the period from 2000 to 2007, *Epidemiology*, 2013, **24**, 23–31.
11 Y. Fang, V. Naik, L. Horowitz and D. L. Mauzerall, Air pollution and associated human mortality: the role of air pollutant emissions, climate change and methane concentration increases from the preindustrial period to present, *Atmos. Chem. Phys.*, 2013, **13**, 1377–1394.
12 K. Meister, C. Johansson and B. Forsberg, Estimated short-term effects of coarse particles on daily mortality in Stockholm, Sweden, *Environ. Health Perspect.*, 2012, **120**, 431–436.
13 R. Guaita, M. Pichiule, T. Maté, C. Linares and J. Díaz, Short-term impact of particulate matter (PM2. 5) on respiratory mortality in Madrid, *Int. J. Environ. Health Res.*, 2011, **21**, 260–274.
14 J. I. Halonen, T. Lanki, T. Yli-Tuomi, P. Tiittanen, M. Kulmala and J. Pekkanen, Particulate air pollution and acute cardiorespiratory hospital admissions and mortality among the elderly, *Epidemiology*, 2009, **20**, 143–153.
15 L. Perez, A. Tobías, X. Querol, J. Pey, A. Alastuey, J. Díaz and J. Sunyer, Saharan dust, particulate matter and cause-specific mortality: A case–crossover study in Barcelona (Spain), *Environ. Int.*, 2012, **48**, 150–155.
16 E. Samoli, R. Peng, T. Ramsay, M. Pipikou, G. Touloumi, F. Dominici, R. Burnett, A. Cohen, D. Krewski and J. Samet, Acute effects of ambient particulate matter on mortality in Europe and North America: results from the APHENA study, *Environ. Health Perspect.*, 2008, **116**, 1480–1486.
17 A. A. Rostami, Computational modeling of aerosol deposition in respiratory tract: a review, *Inhalation Toxicol.*, 2009, **21**, 262–290.
18 N. Tlotleng, T. Kootbodien, K. Wilson, F. Made, A. Mathee, V. Ntlebi, S. Kgalamono, M. Mokone, K. Du Preez and N. Naicker, Prevalence of respiratory health symptoms among landfill waste recyclers in the city of Johannesburg, South Africa, *Int. J. Environ. Res. Public Health*, 2019, **16**, 4277.
19 A. Stobnicka-Kupiec, M. Gołofit-Szymczak, M. Cyprowski and R. L. Górny, Detection and identification of potentially infectious gastrointestinal and respiratory viruses at workplaces of wastewater treatment plants with viability qPCR/RT-qPCR, *Sci. Rep.*, 2022, **12**, 4517.
20 T. M. De Kok, H. A. Driece, J. G. Hogervorst and J. J. Briedé, Toxicological assessment of ambient and traffic-related particulate matter: a review of recent studies, *Mutat. Res. - Rev. Mutat. Res.*, 2006, **613**, 103–122.
21 J. Madureira, I. Paciência and E. D. O. Fernandes, Levels and indoor–outdoor relationships of size-specific particulate

matter in naturally ventilated Portuguese schools, *J. Toxicol. Environ. Health, Part A*, 2012, **75**, 1423–1436.
22 C. Misra, M. D. Geller, P. Shah, C. Sioutas and P. A. Solomon, Development and Evaluation of a Continuous Coarse (PM10–PM25) Particle Monitor, *J. Air Waste Manage. Assoc.*, 2001, **51**, 1309–1317.
23 T. Feng, Y. Sun, Y. Shi, J. Ma, C. Feng and Z. Chen, Air pollution control policies and impacts: A review, *Renewable Sustainable Energy Rev.*, 2024, **191**, 114071.
24 R. Esworthy, *Air Quality: EPA's 2013 Changes to the Particulate Matter (PM) Standard*, Library of Congress, Congressional Research Service, Washington, DC, USA, 2013.
25 D. A. Glencross, T.-R. Ho, N. Camina, C. M. Hawrylowicz and P. E. Pfeffer, Air pollution and its effects on the immune system, *Free Radical Biol. Med.*, 2020, **151**, 56–68.
26 J. O. Anderson, J. G. Thundiyil and A. Stolbach, Clearing the air: a review of the effects of particulate matter air pollution on human health, *J. Med. Toxicol.*, 2012, **8**, 166–175.
27 S. Garg, P. Kumar, V. Mishra, R. Guijt, P. Singh, L. F. Dumée and R. S. Sharma, A review on the sources, occurrence and health risks of per–/poly-fluoroalkyl substances (PFAS) arising from the manufacture and disposal of electric and electronic products, *J. Water Process Eng.*, 2020, **38**, 101683.
28 T. Stoiber, S. Evans and O. V. Naidenko, Disposal of products and materials containing per-and polyfluoroalkyl substances (PFAS): A cyclical problem, *Chemosphere*, 2020, **260**, 127659.
29 A. Voliotis, S. Bezantakos, A. Besis, Y. Shao and C. Samara, Mass dose rates of particle-bound organic pollutants in the human respiratory tract: Implications for inhalation exposure and risk estimations, *Int. J. Hyg. Environ. Health*, 2021, **234**, 113710.
30 K.-H. Kim, S. A. Jahan, E. Kabir and R. J. Brown, A review of airborne polycyclic aromatic hydrocarbons (PAHs) and their human health effects, *Environ. Int.*, 2013, **60**, 71–80.
31 D. Belpomme, P. Irigaray, L. Hardell, R. Clapp, L. Montagnier, S. Epstein and A. J. Sasco, The multitude and diversity of environmental carcinogens, *Environ. Res.*, 2007, **105**, 414–429.
32 A. Besis, D. Voutsa and C. Samara, Atmospheric occurrence and gas-particle partitioning of PBDEs at industrial, urban and suburban sites of Thessaloniki, northern Greece: implications for human health, *Environ. Pollut.*, 2016, **215**, 113–124.
33 Z. Cao, F. Xu, A. Covaci, M. Wu, H. Wang, G. Yu, B. Wang, S. Deng, J. Huang and X. Wang, Distribution patterns of brominated, chlorinated, and phosphorus flame retardants with particle size in indoor and outdoor dust and implications for human exposure, *Environ. Sci. Technol.*, 2014, **48**, 8839–8846.
34 W. Wang, M.-J. Huang, F.-Y. Wu, Y. Kang, H.-S. Wang, K. C. Cheung and M. H. Wong, Risk assessment of bioaccessible organochlorine pesticides exposure via indoor and outdoor dust, *Atmos. Environ.*, 2013, **77**, 525–533.
35 A. L. Moreno-Ríos, L. P. Tejeda-Benítez and C. F. Bustillo-Lecompte, Sources, characteristics, toxicity, and control of ultrafine particles: An overview, *Geosci. Front.*, 2022, **13**, 101147.
36 M. Ho, K.-Y. Wu, H.-M. Chein, L.-C. Chen and T.-J. Cheng, Pulmonary toxicity of inhaled nanoscale and fine zinc oxide particles: mass and surface area as an exposure metric, *Inhalation Toxicol.*, 2011, **23**, 947–956.
37 W.-S. Cho, R. Duffin, S. E. Howie, C. J. Scotton, W. A. Wallace, W. MacNee, M. Bradley, I. L. Megson and K. Donaldson, Progressive severe lung injury by zinc oxide nanoparticles; the role of Zn 2+ dissolution inside lysosomes, *Part. Fibre Toxicol.*, 2011, **8**, 1–16.
38 A. Srinivas, P. J. Rao, G. Selvam, A. Goparaju, B. P. Murthy and N. P. Reddy, Oxidative stress and inflammatory responses of rat following acute inhalation exposure to iron oxide nanoparticles, *Hum. Exp. Toxicol.*, 2012, **31**, 1113–1131.
39 J. Wang and Y. Fan, Lung injury induced by TiO2 nanoparticles depends on their structural features: size, shape, crystal phases, and surface coating, *Int. J. Mol. Sci.*, 2014, **15**, 22258–22278.
40 P. Rajsekhar, G. Selvam, A. Goparaju, P. B. Murthy and P. N. Reddy, Pulmonary responses of manufactured ultrafine aluminum oxide particles upon repeated exposure by inhalation in rats, *Indian J. Forensic Med. Toxicol.*, 2014, **8**, 97–102.
41 W.-S. Cho, R. Duffin, F. Thielbeer, M. Bradley, I. L. Megson, W. MacNee, C. A. Poland, C. L. Tran and K. Donaldson, Zeta potential and solubility to toxic ions as mechanisms of lung inflammation caused by metal/metal oxide nanoparticles, *Toxicol. Sci.*, 2012, **126**, 469–477.
42 G. S. Kang, P. A. Gillespie, A. Gunnison, H. Rengifo, J. Koberstein and L.-C. Chen, Comparative pulmonary toxicity of inhaled nickel nanoparticles; role of deposited dose and solubility, *Inhalation Toxicol.*, 2011, **23**, 95–103.
43 C.-S. Wang, *Inhaled particles*, Elsevier, 2005.
44 W. C. Hinds, *Aerosol technology, properties, behavior, and measurements of airborne particles*, Wiley Interscience, 1999.
45 H. G. Folkesson, M. A. Matthay, B. Westrom, K. J. Kim, B. W. Karlsson and R. H. Hastings, Alveolar epithelial clearance of protein, *J. Appl. Physiol.*, 1996, **80**, 1431–1445.
46 X. M. Zeng, G. P. Martin and C. Marriott, *Particulate interactions in dry powder formulation for inhalation*, CRC Press, 2000.
47 A. J. Hickey, *Pharmaceutical inhalation aerosol technology*, CRC Press, 2003.
48 G. Pilcer and K. Amighi, Formulation strategy and use of excipients in pulmonary drug delivery, *Int. J. Pharm.*, 2010, **392**, 1–19.
49 T. C. Carvalho, J. I. Peters and R. O. Williams III, Influence of particle size on regional lung deposition–what evidence is there?, *Int. J. Pharm.*, 2011, **406**, 1–10.
50 F. Wang, J. Liu and H. Zeng, Interactions of particulate matter and pulmonary surfactant: Implications for human health, *Adv. Colloid Interface Sci.*, 2020, **284**, 102244.

51 L. Jin, X. Luo, P. Fu and X. Li, Airborne particulate matter pollution in urban China: a chemical mixture perspective from sources to impacts, *Natl. Sci. Rev.*, 2017, **4**, 593–610.
52 A. Valavanidis, K. Fiotakis and T. Vlachogianni, Airborne particulate matter and human health: toxicological assessment and importance of size and composition of particles for oxidative damage and carcinogenic mechanisms, *J. Environ. Sci. Health, Part C: Environ. Carcinog. Ecotoxicol. Rev.*, 2008, **26**, 339–362.
53 M. Hussain, P. Madl and A. Khan, Lung deposition predictions of airborne particles and the emergence of contemporary diseases, Part-I, *Health*, 2011, **2**, 51–59.
54 E. R. Weibel, A. F. Cournand and D. W. Richards, *Morphometry of the human lung*, Springer, 1963.
55 T. Soong, P. Nicolaides, C. Yu and S. Soong, A statistical description of the human tracheobronchial tree geometry, *Respir. Physiol.*, 1979, **37**, 161–172.
56 J. Heyder and G. Rudolf, Mathematical models of particle deposition in the human respiratory tract, *J. Aerosol Sci.*, 1984, **15**, 697–707.
57 W. Hofmann, Modelling inhaled particle deposition in the human lung—A review, *J. Aerosol Sci.*, 2011, **42**, 693–724.
58 H. Smith, Human respiratory tract model for radiological protection, ICRP Publication 66, *Ann. ICRP*, 1994, 24.
59 F. Paquet, G. Etherington, M. R. Bailey, R. W. Leggett, J. Lipsztein, W. Bolch, K. F. Eckerman and J. D. Harrison, ICRP Publication 130: Occupational Intakes of Radionuclides: Part 1, *Ann. ICRP*, 2015, **44**, 5–188.
60 N. C. o. R. Protection and Measurements, 1997.
61 C. Yu and C. Diu, Total and regional deposition of inhaled aerosols in humans, *J. Aerosol Sci.*, 1983, **14**, 599–609.
62 W. Nixon and M. Egan, Modelling study of regional deposition of inhaled aerosols with special reference to effects of ventilation asymmetry, *J. Aerosol Sci.*, 1987, **18**, 563–579.
63 C. Darquenne and M. Paiva, One-dimensional simulation of aerosol transport and deposition in the human lung, *J. Appl. Physiol.*, 1994, **77**, 2889–2898.
64 C. Mitsakou, C. Helmis and C. Housiadas, Eulerian modelling of lung deposition with sectional representation of aerosol dynamics, *J. Aerosol Sci.*, 2005, **36**, 75–94.
65 H. C. Yeh and G. M. Schum, Models of human lung airways and their application to inhaled particle deposition, *Bull. Math. Biol.*, 1980, **42**, 461–480.
66 T. Martonen, Analytical model of hygroscopic particle behavior in human airways, *Bull. Math. Biol.*, 1982, **44**, 425–442.
67 B. Asgharian, W. Hofmann and R. Bergmann, Particle deposition in a multiple-path model of the human lung, *Aerosol Sci. Technol.*, 2001, **34**, 332–339.
68 W. Hofmann, B. Asgharian and R. Winkler-Heil, Modeling intersubject variability of particle deposition in human lungs, *J. Aerosol Sci.*, 2002, **33**, 219–235.
69 L. Koblinger and W. Hofmann, Monte Carlo modeling of aerosol deposition in human lungs. Part I: Simulation of particle transport in a stochastic lung structure, *J. Aerosol Sci.*, 1990, **21**, 661–674.
70 W. Hofmann and L. Koblinger, Monte Carlo modeling of aerosol deposition in human lungs. Part II: Deposition fractions and their sensitivity to parameter variations, *J. Aerosol Sci.*, 1990, **21**, 675–688.
71 Z. Zhang, C. Kleinstreuer and C. Kim, Cyclic micron-size particle inhalation and deposition in a triple bifurcation lung airway model, *J. Aerosol Sci.*, 2002, **33**, 257–281.
72 Z. Zhang, C. Kleinstreuer and C. Kim, Flow structure and particle transport in a triple bifurcation airway model, *J. Fluids Eng.*, 2001, **123**, 320–330.
73 J. Comer, C. Kleinstreuer and Z. Zhang, Flow structures and particle deposition patterns in double-bifurcation airway models. Part 1. Air flow fields, *J. Fluid Mech.*, 2001, **435**, 25–54.
74 Z. Zhang, C. Kleinstreuer and C. S. Kim, Airflow and nanoparticle deposition in a 16-generation tracheobronchial airway model, *Ann. Biomed. Eng.*, 2008, **36**, 2095–2110.
75 B. Ma, V. Ruwet, P. Corieri, R. Theunissen, M. Riethmuller and C. Darquenne, CFD simulation and experimental validation of fluid flow and particle transport in a model of alveolated airways, *J. Aerosol Sci.*, 2009, **40**, 403–414.
76 B. Asgharian, R. Wood and R. Schlesinger, Empirical modeling of particle deposition in the alveolar region of the lungs: a basis for interspecies extrapolation, *Fundam. Appl. Toxicol.*, 1995, **27**, 232–238.
77 S. Anjilvel and B. Asgharian, A multiple-path model of particle deposition in the rat lung, *Fundam. Appl. Toxicol.*, 1995, **28**, 41–50.
78 F. J. Miller, B. Asgharian, J. D. Schroeter and O. Price, Improvements and additions to the multiple path particle dosimetry model, *J. Aerosol Sci.*, 2016, **99**, 14–26.
79 W. Hofmann and L. Koblinger, Monte Carlo modeling of aerosol deposition in human lungs. Part III: Comparison with experimental data, *J. Aerosol Sci.*, 1992, **23**, 51–63.
80 A. Afantitis, G. Melagraki, P. Isigonis, A. Tsoumanis, D. D. Varsou, E. Valsami-Jones, A. Papadiamantis, L.-J. A. Ellis, H. Sarimveis and P. Doganis, NanoSolveIT Project: Driving nanoinformatics research to develop innovative and integrated tools for in silico nanosafety assessment, *Comput. Struct. Biotechnol. J.*, 2020, **18**, 583–602.
81 N. Cheimarios, S. Harrison, A. C. Ø. Jensen, P. Karatzas, A. Tsoumanis, P. Doganis, P. Tsiros, D. A. Winkler, S. Lofts and K. A. Jensen, in *Handbook of Functionalized Nanomaterials*, Elsevier, 2021, pp. 81–120.
82 N. Cheimarios, B. Pem, A. Tsoumanis, K. Ilić, I. V. Vrček, G. Melagraki, D. Bitounis, P. Isigonis, M. Dusinska and I. Lynch, An in vitro dosimetry tool for the numerical transport modeling of engineered nanomaterials powered by the Enalos RiskGONE Cloud Platform, *Nanomaterials*, 2022, **12**, 3935.
83 D. G. Mintis, N. Cheimarios, A. Tsoumanis, A. G. Papadiamantis, N. W. van den Brink, H. J. van Lingen, G. Melagraki, I. Lynch and A. Afantitis, NanoBioAccumulate: Modelling the uptake and bioaccumulation of nanomaterials in soil and aquatic invertebrates via the Enalos DIAGONAL Cloud Platform, *Comput. Struct. Biotechnol. J.*, 2024, **25**, 243–255.

84 C. Papavasiliou, D. G. Mintis, A. Tsoumanis, A. Karaoli, I. Lynch, S. Krause, D. D. Varsou, G. Melagraki, M. Kavousanakis and A. Afantitis, MicroPlasticFate web application: Multimedia environmental fate modelling of microplastic particles via the enalos cloud platform, *Bioresour. Technol. Rep.*, 2025, 102157.

85 J. Subbotina, P. D. Kolokathis, A. Tsoumanis, N. K. Sidiropoulos, I. Rouse, I. Lynch, V. Lobaskin and A. Afantitis, UANanoDock: A Web-Based UnitedAtom Multiscale Nanodocking Tool for Predicting Protein Adsorption onto Nanoparticles, *J. Chem. Inf. Model.*, 2025, **65**, 3142–3153.

86 P. D. Kolokathis, E. Voyiatzis, N. K. Sidiropoulos, A. Tsoumanis, G. Melagraki, K. Tämm, I. Lynch and A. Afantitis, ASCOT: a web tool for the digital construction of energy minimized Ag, CuO, TiO2 spherical nanoparticles and calculation of their atomistic descriptors, *Comput. Struct. Biotechnol. J.*, 2024, **25**, 34–46.

87 P. D. Kolokathis, N. K. Sidiropoulos, D. Zouraris, D.-D. Varsou, D. G. Mintis, A. Tsoumanis, F. Dondero, T. E. Exner, H. Sarimveis and E. Chaideftou, Easy-MODA: Simplifying standardised registration of scientific simulation workflows through MODA template guidelines powered by the Enalos Cloud Platform, *Comput. Struct. Biotechnol. J.*, 2024, **25**, 256–268.

88 D.-D. Varsou, P. D. Kolokathis, M. Antoniou, N. K. Sidiropoulos, A. Tsoumanis, A. G. Papadiamantis, G. Melagraki, I. Lynch and A. Afantitis, In silico assessment of nanoparticle toxicity powered by the Enalos Cloud Platform: Integrating automated machine learning and synthetic data for enhanced nanosafety evaluation, *Comput. Struct. Biotechnol. J.*, 2024, **25**, 47–60.

89 D.-D. Varsou, L.-J. A. Ellis, A. Afantitis, G. Melagraki and I. Lynch, Ecotoxicological read-across models for predicting acute toxicity of freshly dispersed versus medium-aged NMs to Daphnia magna, *Chemosphere*, 2021, **285**, 131452.

90 M. Guo, Y. Lyu, T. Xu, B. Yao, W. Song, M. Li, X. Yang, T. Cheng and X. Li, Particle size distribution and respiratory deposition estimates of airborne perfluoroalkyl acids during the haze period in the megacity of Shanghai, *Environ. Pollut.*, 2018, **234**, 9–19.

91 H. Lin, J.-Y. Lao, Q. Wang, Y. Ruan, Y. He, P. K. Lee, K. M. Leung and P. K. Lam, Per-and polyfluoroalkyl substances in the atmosphere of waste management infrastructures: Uncovering secondary fluorotelomer alcohols, particle size distribution, and human inhalation exposure, *Environ. Int.*, 2022, **167**, 107434.

92 EPA, *Multiple-path particle dosimetry (MPPD) model: U.S. EPA technical support documentation and user's guide*, MPPD EPA, China, 2021.

93 O. Price, B. Asgharian, F. Miller, F. Cassee and R. de Winter-Sorkina, *Multiple Path Particle Dosimetry model (MPPD v1.0): A model for human and rat airway particle dosimetry*, RIVM rapport 650010030, 2002.

94 K. Zhang, B.-Z. Zhang, S.-M. Li, C. S. Wong and E. Y. Zeng, Calculated respiratory exposure to indoor size-fractioned polycyclic aromatic hydrocarbons in an urban environment, *Sci. Total Environ.*, 2012, **431**, 245–251.

95 M. Stäuble and H.-J. Schumacher, *ZK Developer's Guide*, Packt Publishing Ltd., 2008.

96 D.-D. Varsou, A. Tsoumanis, A. Afantitis and G. Melagraki, Enalos cloud platform: Nanoinformatics and cheminformatics tools, *Ecotoxicological QSARs*, 2020, pp. 789–800.

97 C. Fuentes, I. Kang, J. Lee, D. Song, M. Sjöö, J. Choi, S. Lee and L. Nilsson, Fractionation and characterization of starch granules using field-flow fractionation (FFF) and differential scanning calorimetry (DSC), *Anal. Bioanal. Chem.*, 2019, **411**, 3665–3674.

98 S. B. Patil and K. K. Sawant, Chitosan microspheres as a delivery system for nasal insufflation, *Colloids Surf., B*, 2011, **84**, 384–389.

99 E. Zora-Guzman and J. R. Guzman-Sepulveda, Optical characterization of native aerosols from e-cigarettes in localized volumes, *Biomed. Opt. Express*, 2024, **15**, 1697–1708.

100 C. Monsé, M. Raulf, B. Jettkant, V. van Kampen, B. Kendzia, L. Schürmeyer, C. E. Seifert, E.-M. Marek, G. Westphal and N. Rosenkranz, Health effects after inhalation of micro-and nano-sized zinc oxide particles in human volunteers, *Arch. Toxicol.*, 2021, **95**, 53–65.

101 S. Zhang, C. Campagne and F. Salaün, Preparation of electrosprayed poly (caprolactone) microparticles based on green solvents and related investigations on the effects of solution properties as well as operating parameters, *Coatings*, 2019, **9**, 84.

102 C. Motzkus, C. Chivas-Joly, E. Guillaume, S. Ducourtieux, L. Saragoza, D. Lesenechal and T. Mace, Characterization of aerosol emitted by the combustion of nanocomposites, *J. Phys.: Conf. Ser.*, 2011, **304**, 012020.

103 A. McDonagh and M. Byrne, A study of the size distribution of aerosol particles resuspended from clothing surfaces, *J. Aerosol Sci.*, 2014, **75**, 94–103.

104 P.-P. Wang, Z.-G. Luo and T. M. Tamer, Effects of octenyl succinic anhydride groups distribution on the storage and shear stability of Pickering emulsions formulated by modified rice starch, *Carbohydr. Polym.*, 2020, **228**, 115389.

105 M. Santa-Maria, H. Scher and T. Jeoh, Microencapsulation of bioactives in cross-linked alginate matrices by spray drying, *J. Microencapsulation*, 2012, **29**, 286–295.

106 O. Werner and C. Turner, Investigation of different particle sizes on superhydrophobic surfaces made by rapid expansion of supercritical solution with in situ laser diffraction (RESS-LD), *J. Supercrit. Fluids*, 2012, **67**, 53–59.

107 Y. Lv, X. Li, T. T. Xu, T. T. Cheng, X. Yang, J. M. Chen, Y. Iinuma and H. Herrmann, Size distributions of polycyclic aromatic hydrocarbons in urban atmosphere: sorption mechanism and source contributions to respiratory deposition, *Atmos. Chem. Phys.*, 2016, **16**, 2971–2983.

108 U.S. New York State Department of Environmental Conservation, *DAR-1: Guidelines for the Evaluation and Control of Ambient Air Contaminants under 6 NYCRR Part 212*, 2020.

109 EFSA, Risk to human health related to the presence of perfluoroalkyl substances in food, *EFSA J.*, 2020, **18**, e06223.
110 U. S. EPA, *Per- and Polyfluoroalkyl Substances (PFAS) Final PFAS National Primary Drinking Water Regulation*, **https://www.epa.gov/sdwa/and-polyfluoroalkyl-substances-pfas**, (accessed June 26, 2025).
111 K. Zhang, B.-Z. Zhang, S.-M. Li, L.-M. Zhang, R. Staebler and E. Y. Zeng, Diurnal and seasonal variability in size-dependent atmospheric deposition fluxes of polycyclic aromatic hydrocarbons in an urban center, *Atmos. Environ.*, 2012, **57**, 41–48.
112 Y. Kawanaka, Y. Tsuchiya, S.-J. Yun and K. Sakamoto, Size distributions of polycyclic aromatic hydrocarbons in the atmosphere and estimation of the contribution of ultrafine particles to their lung deposition, *Environ. Sci. Technol.*, 2009, **43**, 6851–6856.
113 P. Fernández, J. O. Grimalt and R. M. Vilanova, Atmospheric gas-particle partitioning of polycyclic aromatic hydrocarbons in high mountain regions of Europe, *Environ. Sci. Technol.*, 2002, **36**, 1162–1168.
114 K. Hytönen, P. Yli-Pirilä, J. Tissari, A. Gröhn, I. Riipinen, K. Lehtinen and J. Jokiniemi, Gas–particle distribution of PAHs in wood combustion emission determined with annular denuders, filter, and polyurethane foam adsorbent, *Aerosol Sci. Technol.*, 2009, **43**, 442–454.
115 G. Shen, W. Wang, Y. Yang, J. Ding, M. Xue, Y. Min, C. Zhu, H. Shen, W. Li and B. Wang, Emissions of PAHs from indoor crop residue burning in a typical rural stove: emission factors, size distributions, and gas– particle partitioning, *Environ. Sci. Technol.*, 2011, **45**, 1206–1212.
116 A. B. Patel, S. Shaikh, K. R. Jain, C. Desai and D. Madamwar, Polycyclic aromatic hydrocarbons: sources, toxicity, and remediation approaches, *Front. Microbiol.*, 2020, **11**, 562813.
117 A. Haritash and C. Kaushik, Biodegradation aspects of polycyclic aromatic hydrocarbons (PAHs): a review, *J. Hazard. Mater.*, 2009, **169**, 1–15.
118 E. Manoli, A. Kouras and C. Samara, Profile analysis of ambient and source emitted particle-bound polycyclic aromatic hydrocarbons from three sites in northern Greece, *Chemosphere*, 2004, **56**, 867–878.
119 E. Manoli, A. Kouras, O. Karagkiozidou, G. Argyropoulos, D. Voutsa and C. Samara, Polycyclic aromatic hydrocarbons (PAHs) at traffic and urban background sites of northern Greece: source apportionment of ambient PAH levels and PAH-induced lung cancer risk, *Environ. Sci. Pollut. Res.*, 2016, **23**, 3556–3568.
120 M. Rehwagen, A. Müller, L. Massolo, O. Herbarth and A. Ronco, Polycyclic aromatic hydrocarbons associated with particles in ambient air from urban and industrial areas, *Sci. Total Environ.*, 2005, **348**, 199–210.
121 J. Zhou, T. Wang, Y. Huang, T. Mao and N. Zhong, Size distribution of polycyclic aromatic hydrocarbons in urban and suburban sites of Beijing, China, *Chemosphere*, 2005, **61**, 792–799.
122 J. Duan, X. Bi, J. Tan, G. Sheng and J. Fu, Seasonal variation on size distribution and concentration of PAHs in Guangzhou city, China, *Chemosphere*, 2007, **67**, 614–622.
123 A. Besis, D. Gallou, A. Avgenikou, E. Serafeim and C. Samara, Size-dependent in vitro inhalation bioaccessibility of PAHs and O/N PAHs-Implications to inhalation risk assessment, *Environ. Pollut.*, 2022, **301**, 119045.
124 H. Guo, S. Lee, K. Ho, X. Wang and S. Zou, Particle-associated polycyclic aromatic hydrocarbons in urban air of Hong Kong, *Atmos. Environ.*, 2003, **37**, 5307–5317.
125 K. Hayakawa, N. Tang, K. Akutsu, T. Murahashi, H. Kakimoto, R. Kizu and A. Toriba, Comparison of polycyclic aromatic hydrocarbons and nitropolycyclic aromatic hydrocarbons in airborne particulates collected in downtown and suburban Kanazawa, Japan, *Atmos. Environ.*, 2002, **36**, 5535–5541.
126 K. Hayakawa, N. Tang, E. G. Nagato, A. Toriba, S. Sakai, F. Kano, S. Goto, O. Endo, K.-I. Arashidani and H. Kakimoto, Long term trends in atmospheric concentrations of polycyclic aromatic hydrocarbons and nitropolycyclic aromatic hydrocarbons: A study of Japanese cities from 1997 to 2014, *Environ. Pollut.*, 2018, **233**, 474–482.
127 J. C. Bonner, Nanoparticles as a potential cause of pleural and interstitial lung disease, *Proc. Am. Thorac. Soc.*, 2010, **7**, 138–141.
128 H. Qiao, W. Liu, H. Gu, D. Wang and Y. Wang, The transport and deposition of nanoparticles in respiratory system by inhalation, *J. Nanomater.*, 2015, **2015**, 394507.
129 N. R. Yacobi, F. Fazllolahi, Y. H. Kim, A. Sipos, Z. Borok, K.-J. Kim and E. D. Crandall, Nanomaterial interactions with and trafficking across the lung alveolar epithelial barrier: implications for health effects of air-pollution particles, *Air Qual., Atmos. Health*, 2011, **4**, 65–78.
130 M. Riediker, D. Zink, W. Kreyling, G. Oberdörster, A. Elder, U. Graham, I. Lynch, A. Duschl, G. Ichihara and S. Ichihara, Particle toxicology and health-where are we?, *Part. Fibre Toxicol.*, 2019, **16**, 1–33.
131 P. Tsiros, N. Cheimarios, A. Tsoumanis, A. Ø. Jensen, G. Melagraki, I. Lynch, H. Sarimveis and A. Afantitis, Towards an in silico integrated approach for testing and assessment of nanomaterials: from predicted indoor air concentrations to lung dose and biodistribution, *Environ. Sci.: Nano*, 2022, **9**, 1282–1297.
132 E. Garcia, M. B. Rice and D. R. Gold, Air pollution and lung function in children, *J. Allergy Clin. Immunol.*, 2021, **148**, 1–14.
133 C. M. Salome, G. G. King and N. Berend, Physiology of obesity and effects on lung function, *J. Appl. Physiol.*, 2010, **108**, 206–211.